Transformation of Amyloid-like Fibers, Formed from an Elastin-Based Biopolymer, into a Hydrogel: An X-ray Photoelectron Spectroscopy and Atomic Force Microscopy Study

R. Flamia,[†] A. M. Salvi,*,[†] L. D'Alessio,[†] J. E. Castle,*,[‡] and A. M. Tamburro*,[†]

Dipartimento di Chimica, Università degli Studi della Basilicata, 85 Via N. Sauro, 85100 Potenza, Italy, and School of Engineering, University of Surrey, Guildford, Surrey GU2 7XH, United Kingdom

Previous studies have revealed the propensity of elastin-based biopolymers to form amyloid-like fibers when dissolved in water. These are of interest when considered as "ancestral units" of elastin in which they represent the simplest sequences in the hydrophobic regions of the general type XxxGlyGlyZzzGly (Xxx, Zzz = Val, Leu). We normally refer to these biopolymers based on elastin or related to elastin units as "elastin-like polypeptides". The requirement of water for the formation of amyloids seems quite interesting and deserves investigation, the water representing the natural transport medium in human cells. As a matter of fact, the "natural" supramolecular organization of elastin is in the form of beaded-string-like filaments and not in the form of amyloids whose "in vivo" deposition is associated with some important human diseases. Our work is directed, therefore, to understanding the mechanism by which such hydrophobic sequences form amyloids and any conditions by which they might regress to a non-amyloid filament. The elastin-like sequence here under investigation is the ValGlyGlyValGly pentapeptide that has been previously analyzed both in its monomer and polymer form. In particular, we have focused our investigation on the apparent stability of amyloids formed from poly(ValGlyGlyValGly), and we have observed these fibers evolving to a hydrogel after prolonged aging in water. We will show how atomic force microscopy can be combined with X-ray photoelectron spectroscopy to gain an insight into the spontaneous organization of an elastin-like polypeptide driven by interfacial interactions. The results are discussed also in light of fractal-like assembly and their implications from a biomedical point of view.

Introduction

There is a great deal of interest in elastin-like polypeptides (ELPs) for their potential use in bioengineering and biomedical applications.

The synthesis and characterization of biopolymers corresponding to repeating sequences of elastin is well established.[1] It has been repeatedly verified that, depending on the given sequences, ELPs show the ability to assume, under "laboratory" control, multiple conformations that recall those of the parent elastin.[1–4] Since this implies similar elastic and biocompatibility characteristics, these polypeptides provide useful models for the comprehension of elastin elasticity, and studies on their sequence–structure relationship can be important for the design of prosthetic biomaterials.[1] Furthermore, some highly hydrophobic polypeptides have a tendency to form amyloid-like fibers when suspended in water,[2,5] and therefore, investigations of their structural features may also contribute to the understanding of amyloid formation.

This fact is extremely important in biomedicine, as it is well-known that these fibers are related to many important human diseases generally known as "amyloidosis".[6] More than 20 human diseases are known to belong to this class, which includes Alzheimer's disease, Creutzfeldt–Jacob syndrome, and type II diabetes (http://www.orpha.net/data/patho/GB/uk-amyloidosis.pdf).

In recent papers[2,7] we have shown how atomic force microscopy (AFM) is valuable, when used in conjunction with X-ray photoelectron spectroscopy (XPS), for the study of the pentapeptide ValGlyGlyValGly in both its monomer and polymer forms. Previous studies on the monomeric sequence had already shown that it exhibited some physicochemical properties of elastin, and in particular, at the supramolecular level, electron microscopy demonstrated extensive aggregation of the pentapeptide to give elastin-like structures such as twisted ropes and banded fibrils.[8]

The polymer form of the same sequence was revealed by XPS and AFM to self-assemble in different supramolecular structures when deposited on a silicon surface from suspension in different solvents. The formation of filamentous structures evolving to beaded strings was found in deposits from methanol suspension and explained with surface energy considerations.[2,7] The structure's stability was examined as a function of time showing that it was achieved through contact, by hydrogen bonds, with the hydroxylated groups on a silicon substrate and also by displacement of preadsorbed surface contaminants. With deposits from suspension in water, the formation of stable and stiff amyloid fibers was reproducibly obtained and explained as being promoted by interchain hydrogen bonds mediated by the water itself.[2,7]

As a step forward for ELP investigations, we describe in this paper the changes in aggregation and structure arising from the full hydration of poly(ValGlyGlyValGly) deposited after a long period of storage in water suspension. A particular consequence of this hydration is the formation of a hydrogel dispersion. This comparison between the amyloid fibers seen in the original deposit and those seen in the deposit from the aged suspension,

* Authors to whom correspondence should be addressed. E-mail: salvi@unibas.it; J.Castle@surrey.ac.uk; tamburro@unibas.it.
† Università degli Studi della Basilicata.
‡ University of Surrey.

undertaken by the techniques of AFM and XPS, focuses attention on the ability of the amyloid fibers to reorganize themselves. Reorganization gives a large increase in their aspect ratio and a much finer and more uniform distribution in the aqueous phase. The uniformity of this aqueous distribution has been confirmed by calculation of the fractal dimension of a poly-(ValGlyGlyValGly) hydrogel from many AFM images using a reliable method.[9]

Experimental Section

Poly(ValGlyGlyValGly) Pentapeptide. The synthesis of both the monomer and the polymer has been described elsewhere.[2] In short, the poly(ValGlyGlyValGly) had a polydispersivity, as determined by matrix-assisted laser desorption ionization mass spectrometry, corresponding to a number of pentameric units in the range of 2−9. As prepared, the material was in the form of a dry powder. It was suspended in deionized water at an equivalent concentration of 1 mg in 1 mL of water (ca. 0.1%), the concentration, unless otherwise specified, which represents the best compromise in accounting for both XPS and AFM sensitivity requirements.[2,7] The fresh suspension was deposited as droplets (a) on a clean silicon substrate taken from a new 100 silicon wafer or (b) on a piece of gold foil (Johnson Matthey, Materials Technology, U. K.) that had been cleaned by etching with a beam of argon ions in the ultra-high-vacuum preparation chamber of the spectrometer. The original poly(ValGlyGlyValGly), which had already been the source of several depositions on silicon surfaces and was therefore well characterized, was left in water suspension for a further period of several months whereupon it transformed spontaneously into the hydrogel form. This material was deposited as a thin smear on the silicon and gold substrates using a clean spatula. At this stage the development of the hydrogel, in particular its dependence on molecular weight and polidispersivity, has not been investigated because of the insolubility or very poor solubility of the polymer in all conventional solvents used for fractionation of polypeptides.

Atomic Force Microscopy. As in past work, the structural study has been carried out by use of an atomic force microscope (Digital Instruments, Multimode and Dimension Instruments) using silicon substrates. The gold foils used for the XPS measurements were not sufficiently smooth for AFM work. All experimental data were collected in tapping mode, using scanner J (scan range 100 μm) and standard Si probes (NT-MDT, Russia). Further details are given in a previous paper.[2] Caution is required to obtain good images: In fact, as soon as the AFM acquisition starts, the tip may pick up material from the sample, becoming dirty, this demonstrating that the polymer is "sticky". Furthermore, when the tip is subjected to fast scans in an attempt to clean it, scratches are likely to form on the sample surface giving edges around which are deposits of broken fibers. Apparently the fibers act as "rubber bands" that gather together around the point of fracture when broken.

Fractal Analysis. The fractal dimension[10] of poly(ValGlyGlyValGly) as a deposit in hydrogel form has been calculated from many AFM images. The procedure requires a preliminary conversion from the initial JPEG image format to a BMP (bitmap) black and white picture, which is needed to distinguish between full structures and empty space. The filtering and enhancing of the images was accomplished with the photo editing software Ulead Photo Express[11] to capture the relevant features of the observed structures. The bitmap pictures were then imported into the Benoit[12] software for calculation of the fractal dimension.

There is no unique definition of fractal dimension, but rather there are a variety of methods used to measure it.[13] The box dimension, based upon the Box Counting Theorem,[14] has the most applications in science. It is defined as the exponent D in the relationship
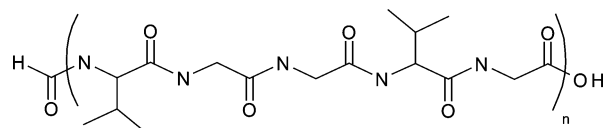
$$N(d) = \frac{k}{d^D}$$

Figure 1. Schematic representation of poly(ValGlyGlyValGly). According to a log-normal distribution of the pentameric units centered on 5, the stoichiometric C/N/O ratio is 3.2:1.0:1.0.[7]

where $N(d)$ is the number of boxes of linear size d necessary to cover a data set of points distributed in a two-dimensional plane. In practice, to measure D, one lays on the set a grid of size d and counts $N(d)$ for a range of values of d, then plots the logarithm of $N(d)$ on the vertical axis versus the logarithm of d on the horizontal axis. If the set is fractal, then this plot will follow a straight line with a negative slope that equals $-D$. In the present case figures obtained by box counting were consistent with the fractal dimensions obtained by other algorithms using perimeter-area information, mass, or ruler methods that can be implemented in the program.

The analysis of images rather than the original data means that the fractal dimension refers to the planar projection of the real structures embedded in the three-dimensional space. The problem of the correlation between the fractal dimension of an object embedded in three dimensions and its plane projection has been addressed by Mandelbrot.[15] If the object is a fractal of dimension D, then the projection will be itself of dimension D provided that D is less than two. This is a consequence of the Projection Theorem, or Shadow Theorem,[16] related to the projection of a fractal in R^n onto a lower-dimensional subspace. All of the images analyzed met this requirement.

X-ray Photoelectron Spectroscopy. The X-ray photoelectron spectra were acquired with a LH X1 Leybold instrument using a double un-monochromatized anode (Al Kα, 1486.6 eV, and Mg Kα, 1253.6 eV) operating at a constant power of 260 W. Wide and detailed spectra were collected using the fixed analyzer transmission (FAT) mode of operation with a pass energy of 50 eV and a channel width of 1.0 and 0.1 eV, respectively: Under these conditions, the instrumental contribution to line width is kept constant. The Au $4f_{7/2}$ (84.0 eV), Cu $2p_{3/2}$ (932.7 eV), and Ag $3d_{5/2}$ (368.2 eV) signals from standard foils were used for calibration purposes.

To allow a meaningful comparison, the samples for XPS should be an exact replica of those imaged by AFM. Accordingly, the silicon pieces used for ELP deposition for both types of analysis were all taken from the same Si(100) wafer. As reported in previous work,[7] the silicon surface was first analyzed by XPS after a prewashing with the solvent used for suspending the polymer so that contributions from the substrate can be taken into account when analyzing the polymer spectra.

Curve-Fitting Program. The acquired X-ray photoelectron spectra were analyzed with Googly, a curve-fitting program fully described in previous work[17,18] and which has the advantage of applying a standard Shirley background[19] to each individual component of a complex peak consisting of several overlapping chemical states. Peak areas were converted to composition in at. % using established procedures and sensitivity factors (SFs) appropriate to our XPS spectrometer.[20a] The procedure used to derive the peak areas is that used for the same polymer sequence in previous work,[7] and to permit comparison, similar energy windows are used for displaying the curve-fitted regions. Similarly, the selected best fits were all required to satisfy the elemental mass balance based on the stoichiometry of the pentapeptide formula (Figure 1), within the limit of XPS accuracy.[20b] The energy scales of the XPS figures reported in this paper are not corrected for surface charging, but the peak assignments (binding energies, BEs), as reported in the text, are referenced to the C 1s aliphatic carbon, as an internal standard, set at 285.0 eV and to literature data. (See refs 20 and 21 and the National Institute of Standards and Technology, Standard Reference Database 20, http://www.nist.gov/srd/surface.htm.)
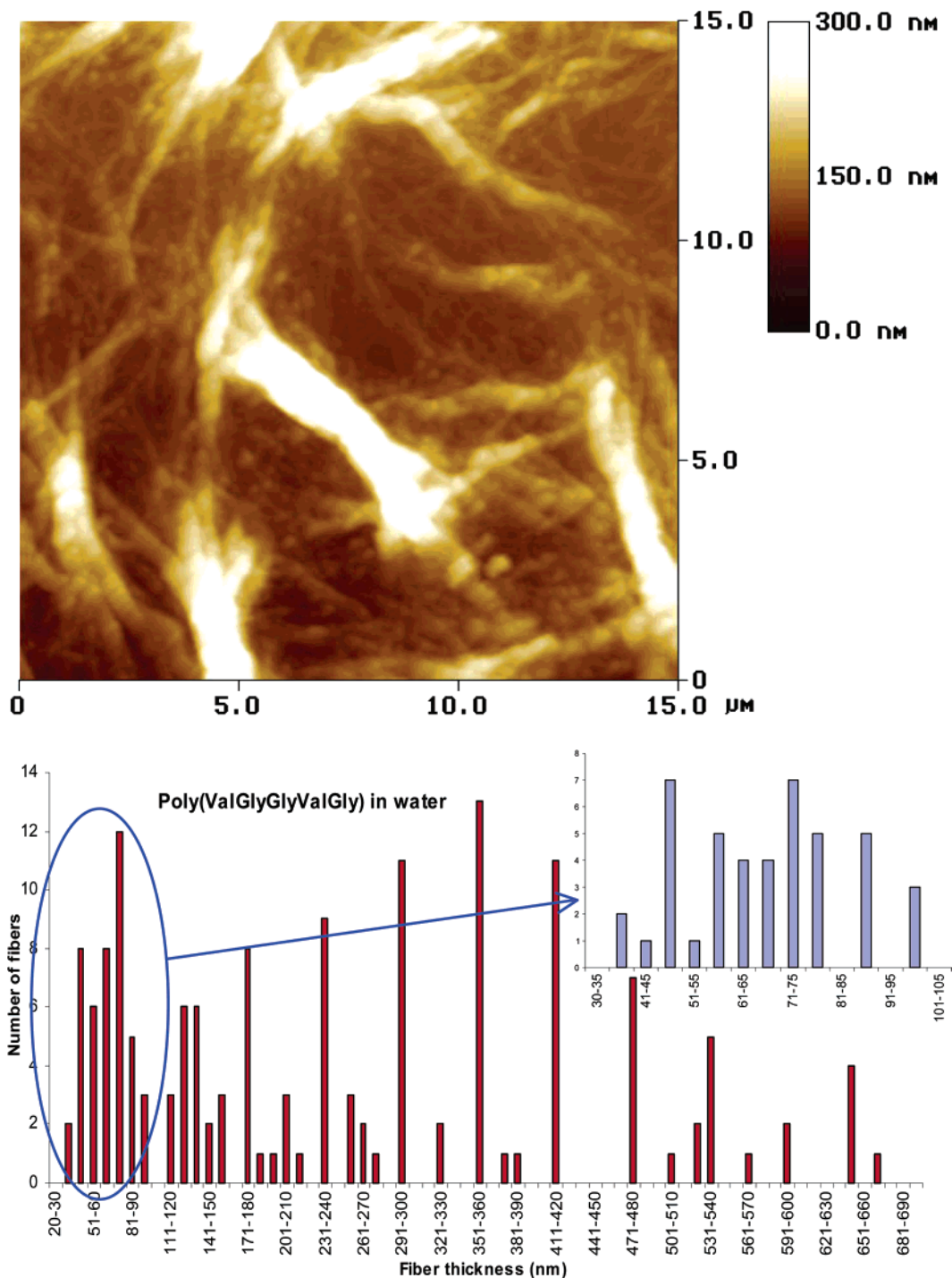
Figure 2. Atomic force micrograph of amyloids deposited from suspension in water and a histogram showing their diameter distribution.

Results

AFM and Fractal Analysis. The ELP, when freshly deposited on a silicon surface from water suspension, has already been described:[2] Images show poorly dispersed clumps of amyloid-like fibers. The amyloid structure seems stable, and the fibers do not evolve to other forms of organization even after days from the samples' preparation (Figure 2). There are two features of particular interest in the context of the present study: First, the fact of the clumping of the fibers suggests that this is a consequence of the hydrophobic character of such fibers, and second, there are multiple layers in the helical structures. The histogram reported in lower part of Figure 2, obtained by analyzing 152 different fibers, shows the populations of the

fibers and fiber clusters, deposited from water suspension, in relation to their aggregation sizes. The first peak in the distribution is in the range of 45−50 nm in diameter, and for clarity, the initial part of the distribution, ranging from 35 to 105 nm, is amplified in 5 nm steps in the inset histogram. Beyond 120 nm the sets of diameters increase in size in a coherent manner, in steps of approximately 60 nm up to a maximum of ca. 600 nm. The typical image shown in Figure 2 shows that many of the larger sizes are made up of bundles of smaller fibers, themselves being helical in structure, that are held together by a wrapping fiber. It seems that the 60 nm diameter fibers aggregate preferentially, producing clusters whose thickness is a multiple of 60 nm. Larger or smaller fibers,
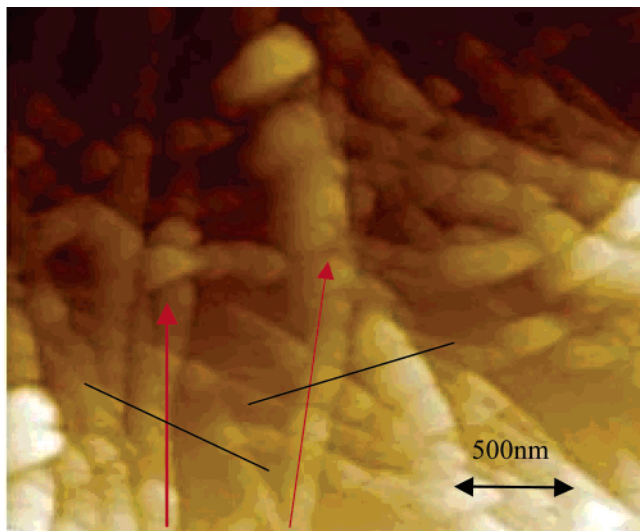
Figure 3. Example of handedness in the wrapping of fiber bundles. Black lines show the helix hand along a fiber axis indicated by the red arrow.

even if present, as demonstrated by the inset histogram, do not preferentially aggregate. In many other cases the bundles are wrapped in a ribbon with a thickness of ca. 10 nm that increases the measured thickness of the bundle by ca. 20 nm.

The pitch of the helix of all these fibers and fiber bundles is generally in the range of 75−85 nm. These images also give information on the relative abundances of the left-handed (LH) and right-handed (RH) helices, and by analyzing several images the LH/RH ratio is found to be 3.5:1. Figure 3 shows examples of the handedness for ribbons in the wrapped bundles in which the differences are particularly clear.

All measurements were performed off-time on previously acquired images; thicker fibers were measured at lower-resolution images, and it is worth noting that in decreasing the resolution of the AFM images the accuracy of the thickness measurement is also decreased. It may be that in the histogram the set of data relative to thicker fibers has a distribution similar to that of the inset set if properly resolved.

Typical images of the spontaneously formed hydrogel are shown in Figure 4. As can be seen from these images, the multiple clustering has disappeared, and the fibers have a high degree of dispersion. The multiple helices have been refined, and the histogram in the lower part of Figure 4, obtained by measuring 110 fibers, now shows nearly a symmetric distribution that gives an overwhelming abundance of long fibers with a diameter range of 46−50 nm. A nice example of a remaining double helix is shown in Figure 5, which shows two amyloid fibers twisting together (at point A) to form a thicker "rope". As before the images were analyzed to identify the LH/RH ratio, but in this case, all of the fibers that could be clearly identified were only showing LH helices. In one case a fiber seems to change the twisting direction from LH to RH, forming an angle of about 270°. (This is pointed out with a green arrow in Figure 6.) This finding may suggest that the twisting started simultaneously from both ends of the fiber.

Figure 6 gives an example of the analysis of fractal dimension and shows the original micrograph, the image after background removal, and the image after transformation to a black and white bitmap. The result of fractal analysis conducted with the box-counting method is also shown. The data are typical of those found from images of the hydrogel, reproducibly, giving a value of $D = 1.8$. This represents a surface ($D = 2$) significantly

covered by structures, in keeping with a visual appreciation of the micrograph, and expected for an extensive hydrogen-bonded hydrogel, in excellent agreement with what has been found for a fully hydrated coacervate of α-elastin.[9,22]

XPS Analysis. In the upper part of Figure 7 are shown the wide spectrum of poly(ValGlyGlyValGly) in the form of hydrogel deposited on silicon and in the inset the C 1s curve-fitted region of the carbon present on substrate surface before the polymer deposition (surface contamination). The wide spectrum also shows the presence of phosphorus (see labels), randomly found in repeat tests and that, going back to the preparative procedures, can be attributed to a contamination of diphenyl phosphorazidate (DPPA) used as a polymerizing agent during the polymer synthesis.[2]

In the lower part of Figure 7 are shown the C 1s curve-fitted regions of the polymer deposited on silicon (a) from a water suspension and (b) from a hydrogel. To resolve the polymer signals in these spectra the surface contamination is included in the fit together with the eventual contribution from synthesis residues (see peak 0 at the lowest BE side) and then subtracted following the procedure already reported in previous work.[7]

The component peaks of the C 1s spectrum of amyloids suspended in water (Figure 7a) already have been assigned,[7] and splitting of the carbonyl amide peak ($>C=O$ at 287.6 eV and $>C=O\cdots H$ at 288.8 eV) due to the formation of intermolecular hydrogen bonds, mediated by the water itself, was identified in previous work.

In the analysis of the hydrogel, using the same curve-fitting procedure, the C 1s spectrum (Figure 7b), after silicon-contamination subtraction, has revealed the presence of three distinct components in an area ratio of 5.8:5.0:5.3 that have been assigned to aliphatic carbons (BE of 285.0 eV), carbons in the α-position in the polymeric chain (BE of 286.4 eV), and $C=O$ groups (BE of 288.1 eV), respectively. The experimental ratio is coincident, within our accuracy, with that estimated from stoichiometry, equal to 6.0:5.0:5.0 for the given peaks.

The primary evidence arising from the fitted peaks of the hydrogel deposit is clearly the lack of splitting for the carbonyl group. Instead, this peak has a binding energy that lies just between the previous split signals as if hydrogen bonds were possibly extended throughout the polypeptide chains and with similar strengths. Further investigation of the carbonyl, using the oxygen peak, was not possible because the signal from the oxygen of the polypeptide is confounded with that originating from oxidized and hydrated silicon layers.[7] Thus, to confirm the importance of hydrogen bonds (and possibly of water) in the stability of the hydrogel network, samples were examined using sputtered gold as a substrate to minimize interference with the oxygen signal.

The upper part of Figure 8 shows that no oxygen is present in the wide spectrum of sputtered gold, and the asymmetry of the carbon peak, due to a residual contamination on its surface, can be fully accounted for by the intrinsic background[23] introduced to the fit using the κ parameter in Googly.[17,18]

The lower part of Figure 8 shows the C 1s, O 1s, and N 1s curve-fitted regions of a poly(ValGlyGlyValGly) hydrogel deposited on a gold surface.

As found for the spectra using the silicon substrate, three components were identified in the carbon signal (in addition to the one belonging to gold contamination that was added with its κ parameter) having area ratios of 6.0:5.0:4.9 and assigned to aliphatic carbons (BE of 285.0 eV), carbons in the α-position (BE of 286.3 eV), and $C=O$ groups (BE of 288.1 eV), respectively. Moreover, in this case, the oxygen signal could
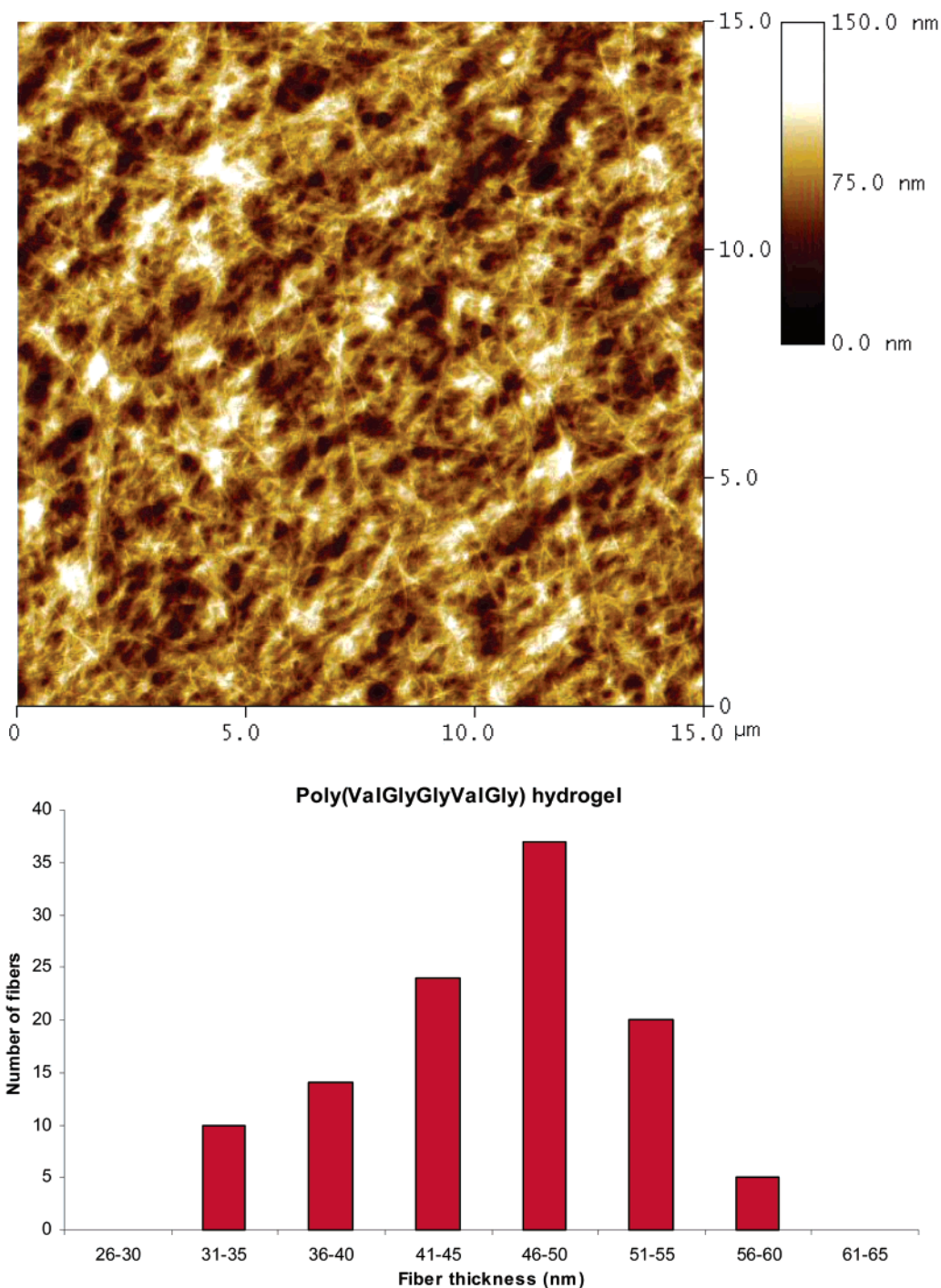
Figure 4. Atomic force micrograph of amyloids deposited from a hydrogel and a histogram showing their diameter distribution.

be resolved into two components: The calculated area of the first one (BE of 531.2 eV) balances that of the carbonyl peak in the carbon region. This peak therefore belongs to the polymer and confirms the only one single state of the C=O groups. The second peak, clearly visible at a BE of approximately 533.0 eV can then only be assigned to water molecules trapped in the hydrogel network.

The nitrogen signal at 400.1 eV also has an area ratio of unity with the peptide >C=O signals and appears as an almost single peak. The binding energy is specific to a peptide amide not involved in hydrogen bonds. (The same was true for nitrogen on a silicon substrate at a BE 400.2 eV, here not reported.) The slight asymmetry at higher BEs could eventually signify a weak involvement, in a hydrogen bond with water, as hydrogen-bond acceptors.

The hydrogel spectra on gold substrates give a C/O/N ratio of 3.2:1.1:1.0, strongly concordant with the theoretical ratio, as always obtained from the fits on silicon. Thus we can be quite confident on the obtained results and are able to propose modeled structures in concordance with AFM results.

The presence of water-promoted hydrogen-bond bridges between polymeric chains was already suggested for explaining the X-ray photoelectron spectra of amyloid fibers suspended in water (Figure 9).[7] These new spectra give evidence for a more ubiquitous presence of water that, logically, would imply a more extensive formation of probably weaker hydrogen bonds contributing to the construction of the hydrogel network (Figure 10). However, the significance of the extended interaction with water will be returned to in the Discussion.
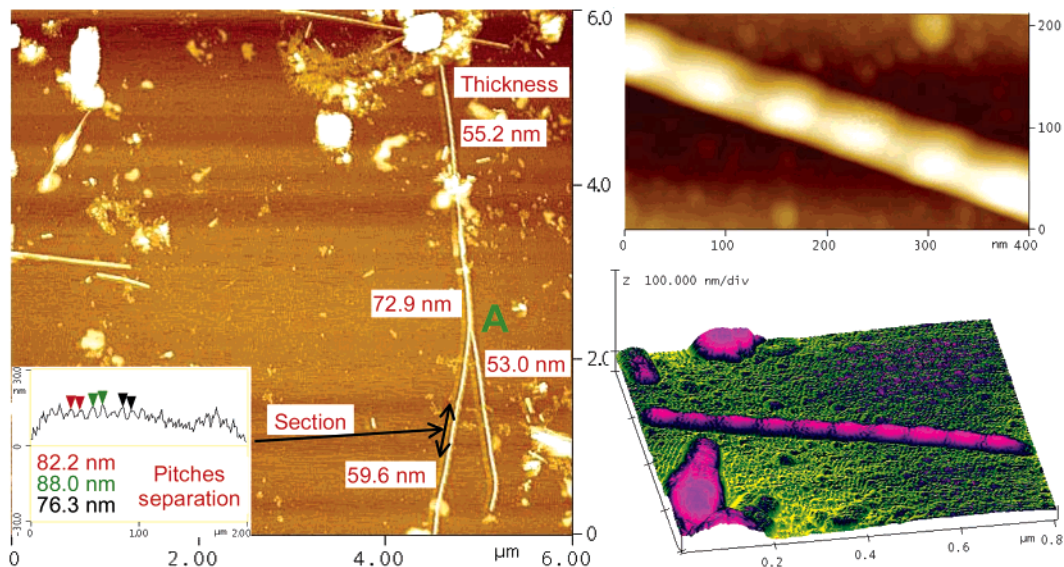
Figure 5. Atomic force micrographs of amyloid fibers deposited from a hydrogel. The inset shows a section taken from the fiber indicated by an arrow. The fiber diameters are also given.
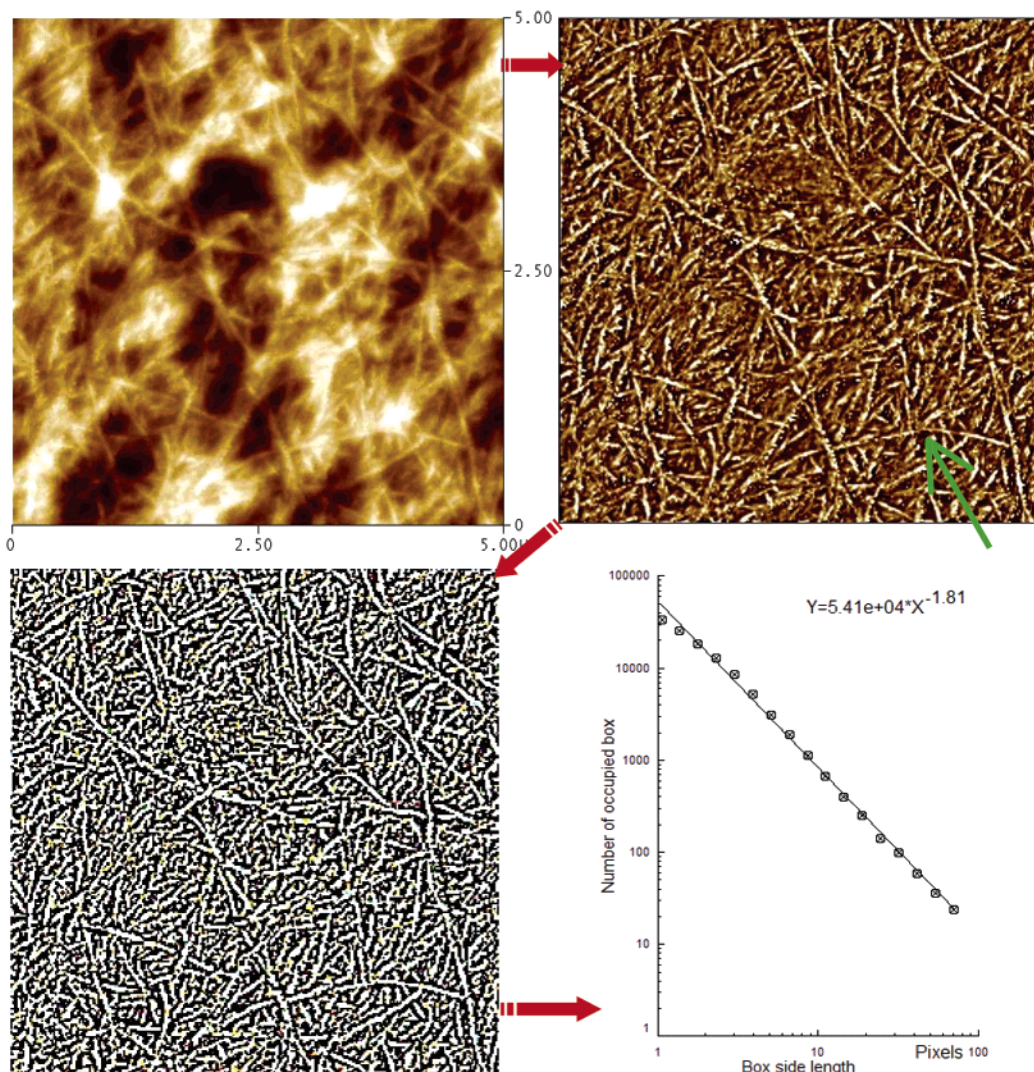

Figure 6. Fractal dimension calculation. The figure shows the original AFM image, the image after background removal, the black and white bitmap, and the fractal analysis conducted by the box-counting method. The green arrow indicates a point in which the fiber passes from left- to right-handed.
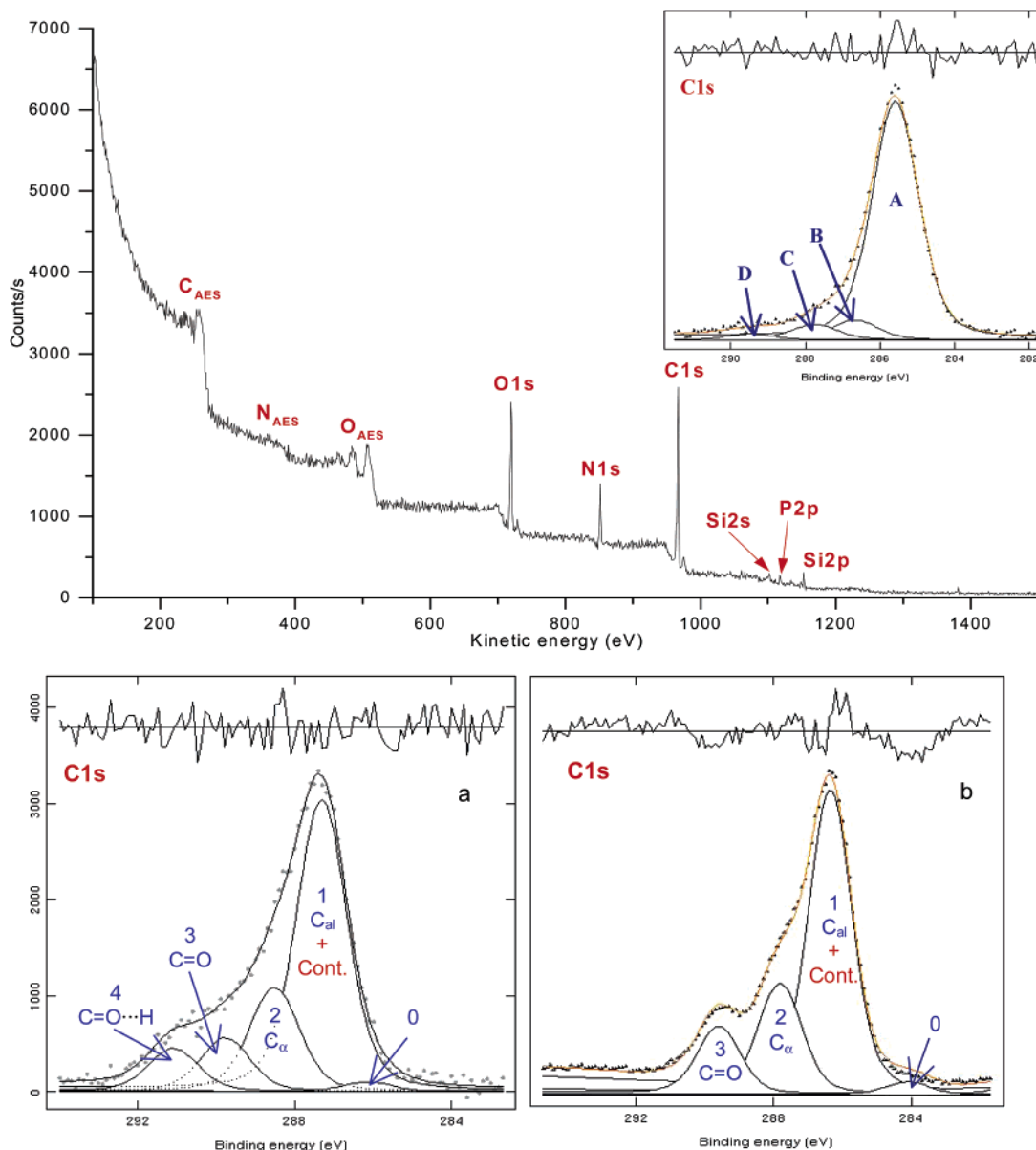
Figure 7. XPS wide scan of the amyloids deposited from suspension in water. The inset shows the C 1s region of the silicon substrate before the deposition: (a) C 1s curve-fitted region of the suspension in water deposited on Si; (b) C 1s region of the hydrogel deposited on Si.

Discussion

Image Analysis. Visual inspection of the ELPs, as deposited from a water suspension (Figure 2), shows a rather chaotic aggregation of fibrous material. Fractal analysis of these images shows evidence of self-similar behavior, also indicated by the patterned distribution in the histogram; however, no meaningful fractal dimension could be extracted. In fact, the multiscale analysis gives $D \approx 1$, thus indicating a linear Euclidean structure, as supported by visual inspection. Some thin fibers can be seen within the images, but other features seem to represent bundles of fibers, in some cases wrapped by a helical structure that can have a LH or a RH spiral.

Observations and measurements made from a large number of images suggest that the basic macromolecular aggregate is in the form of a flat ribbon. This ribbon twists into a helix with a diameter in the range of 45−60 nm, although helices with a diameter of approximately 60 nm appear to be the most common feature giving rise to most, if not all, of the observed structures. For example, from a size of 180 nm onward, the most probable sizes occur at intervals of 60 nm. This suggests that the bundles

and ropes are formed from clusters of fibers having the basic 60 nm helical structure. Examples of possible close-packed clusters are shown in Figure 11a. The maximum probability for the size distribution (at ca. 360 nm) would correspond to 37 single fibers of 60 nm in diameter. That even greater diameters are found in the distribution shows that much larger numbers of fibers are clustered together in some of the bundles.

No evidence is found in the images for the isolated flat ribbons. Observation of the images, such as Figure 5 (taken, for clarity, from the set of hydrogel images), suggests that this arises because any ribbons that have not spiralled into a helix have a tendency to wrap around another helix, using this as a template. In this way multiple layers can form, as illustrated in Figure 11b. In Figure 5, the junction at point A is between two individual fibers, and since fibers usually do not bend, the fiber starting on the top of the image continues from top to bottom. The proposed structure of the overlap is sketched in Figure 11c.

There are two possible interpretations concerning the fiber forming the spur at point A, although both lead to the same important conclusion. Either the junction was formed during
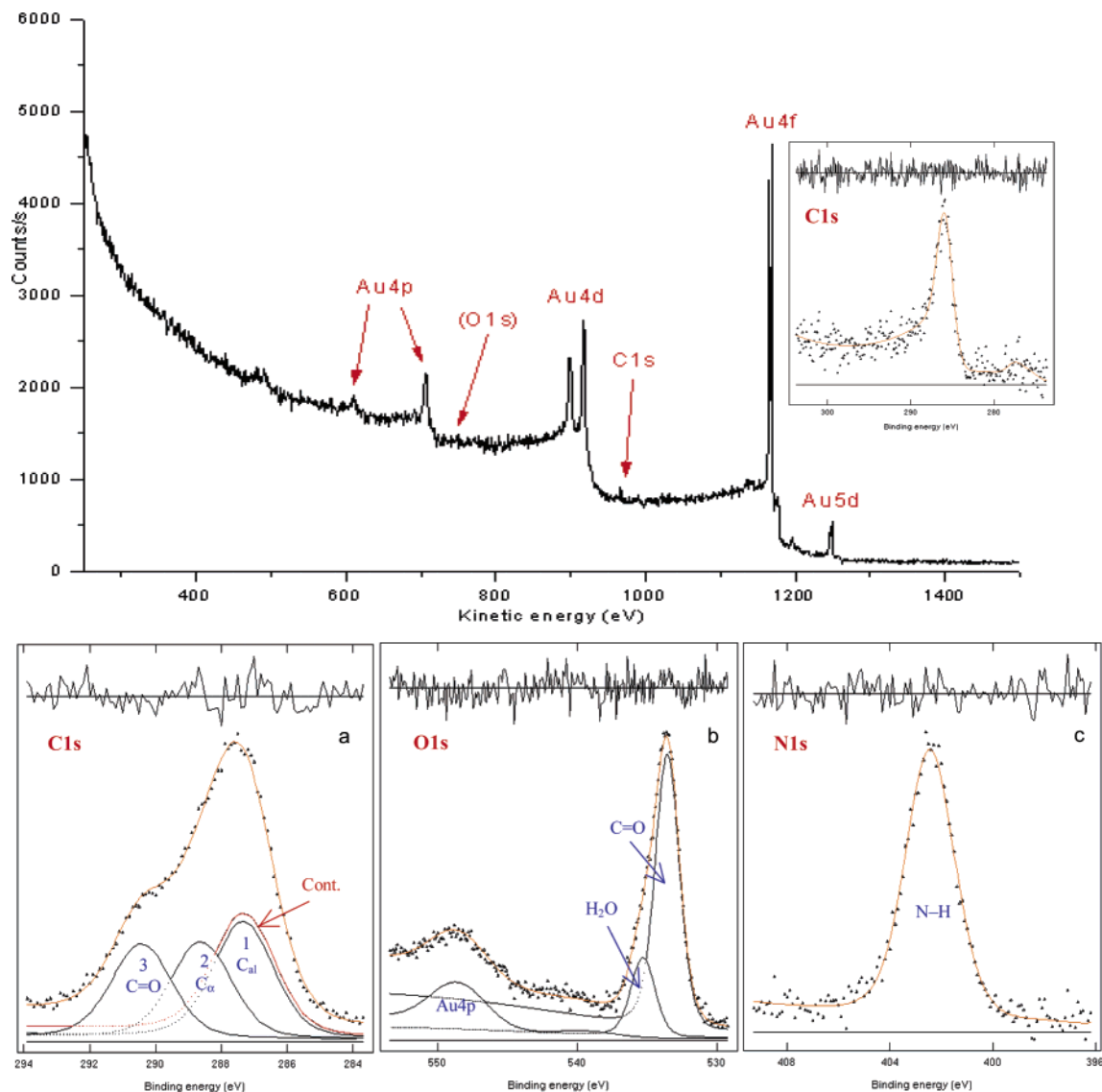
Figure 8. XPS wide scan of gold substrate. The inset shows the C 1s region before the deposition: (a) C 1s, (b) O 1s, and (c) N 1s curve-fitted regions of the hydrogel deposited on gold.
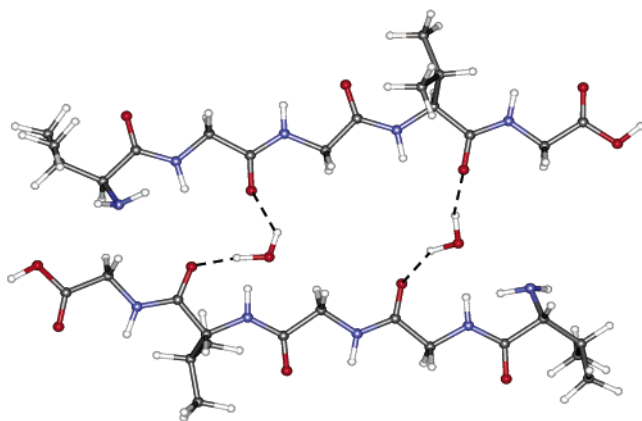

Figure 9. Model for the interaction of poly(ValGlyGlyValGly) with water.

Figure 10. Model for the extensive interaction of the poly(ValGlyG-lyValGly) hydrogel with water.

amyloid formation, in which case the one on the left, while it is wrapping on itself, encounters the other one, at point A, and starts to wrap on that or the two fibers are separating, leaving a distance of approximately 1.5 μm in which one fiber is still spiralled around the other. The diameter of the overlapped region, as indicated in Figure 5, reaches 73 nm, whereas the
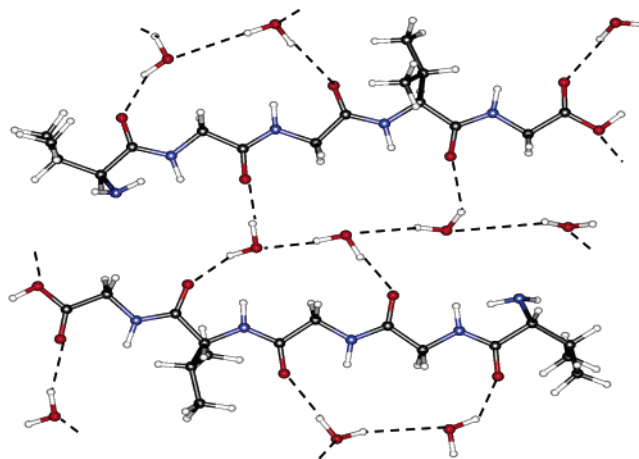
single fibers are between 53 and 60 nm. It is this type of image that has been used to obtain the dimensions of the pre-amyloid ribbon from which all of the structures are formed: The increase in diameter corresponds to a thickness of between 6.5 and 10 nm, and the pitch of the helix shows it to have a width of ca.
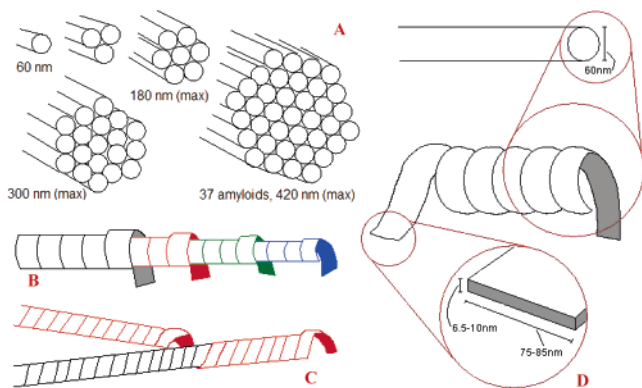
Figure 11. Amyloid models: (A) aggregation of 60-nm-thick fibers; (B) formation of a fiber by wrapping ribbons on template structures; (C) schematic illustration of the fibers shown in Figure 3; (D) ribbon, helix, fiber.

80 nm. Each layer increases the diameter of the helical structure by $15-20$ nm, and it is this that gives rise to the close spacing seen in the size distribution below 120 nm as given in the inset histogram of Figure 2. Many examples of this behavior were seen in the images, and in some cases the outer ribbon wraps together bundles of fibers. The nature of the overlap in Figure 5 also leaves no possibility for the presence of an inner core to the amyloid structure, and we conclude that the amyloid fibers are hollow. Figure 11d gives an indication of the structure of the basic amyloid fiber seen throughout the studied material.

Turning now to the size distribution found in the images of the hydrogel (Figure 4), it is seen that the evidence for clustering is no longer present, and although there is some remaining evidence for double layering within a given helix, as has already been pointed out in Figure 5, most of the multiple layers have disappeared along with the RH spirals found in some of the outer ribbons. The changes are associated with an apparent increase in length and decrease in diameter of individual amyloid fibers. Thus the dispersion of fibers is complete, as illustrated by the fractal behavior of all hydrogel images, typified by that given in Figure 6. The process of change is, however, slow: Images such as that in Figure 2 were quite stable over many days. We can assume, from the very high and uniform level of dispersion in the hydrogel, that the fibers are fully hydrated whereas the clumping observed in the original deposits shows that they were originally excluded from the solvents because of hydrophobic self-interactions.

The refinement of the fibers that leads to formation of the hydrogel moves in a contrary direction to the formation of multiple helices. Presumably by a process of reptation, the higher layers move to the end of the template fiber and thus extend its length: The clumps of fibers unravel, and individual strands separate and randomize. Such behavior is consistent with the hydration of the ELP surface, and again water seems to play its role. The resultant, long, amyloid-like fibers are stiff showing little evidence of sharp curves and bend very little when passing over each other at points of intersection (Figure 5). It looks as if a three-dimensional hydrogen-bonded network has formed at the cost of the entropic gain that is normally the origin of hydrophobic attraction.[24] Thus the process that has allowed the dispersion of the amyloid fibers is likely to have been hydration of their outer surface.

Surface Chemical Analysis. We have previously proposed[2,7] that water is an important mediator of the amyloid structure, allowing the formation of hydrogen-bonded bridges as shown in the computer structure of Figure 9. The formation of multiple layers, the innermost acting as a template for each successive

helix, could be driven by hydrogen-bond formation, but it equally serves to reduce the surface area exposed to "bulk" water and thus acts to minimize the free energy of the system of water and hydrophobic fibers. The result would imply some water to be confined between helices cooperating through bilateral hydrogen bonds in the formation of amyloid aggregations.

Neither AFM nor XPS are able to detect individual molecules within the ribbons and helices, and nothing can be said, therefore, on how they are packed within these structures. Nevertheless, XPS measurements of hydrogel deposits on a gold substrate show, in the oxygen spectrum, clear evidence for the presence of water within the structure. Also, the key elements of the polymer chains have only one chemical state (no splits in their binding energies) as if they all experience the same environment. Thus XPS supports the view that there is a very uniform hydration environment throughout the molecular structure, as in the attempted representation of such a uniform distribution of water around the polypeptide chains in the computer-generated image in Figure 10.

However, some relevant details from the XPS investigation should be emphasized. First, the carbon signal of the peptide groups has a binding energy that is intermediate, between the nonbonded and the hydrogen-bonded carbon of the polymer and the polymer suspension.[7] Second, from the experiments on gold with the hydrogel, the nitrogen and oxygen BEs are found to be practically coincident and even lower in the case of oxygen than those corresponding to a nonbonded peptide in the powdered polymer.[7] The experiments on silicon, here and in previous work,[7] confirm this result for nitrogen (although not for oxygen, because of the hydroxyl's influence on oxygen from silicon surfaces, as already mentioned). Thus, the effect of "extended" hydrogen bonds that should mainly involve oxygen (and nitrogen) moieties seems to propagate more on the peptide carbon.

To have a confirmation on these findings and to verify if differences in chemical states could be demonstrated and eventually related to the different nature of the substrates, supplementary XPS experiments have also been performed by depositing the polymer suspended in water onto the gold substrate. As can be demonstrated from Figure 12, after being prewashed with water, similarly to what is encountered on a silicon substrate, organic contaminants give additional components in the spectral regions, and particularly, the O 1s spectra are further complicated by the presence of water (see insets). Minor differential charging was also demonstrated between the signals from gold and those from the polymer (in the range of $0.2-0.4$ eV); however, the final important outcome is that these supplementary results confirm and extend our previous findings on amyloids. In particular, starting with the right C/O/N ratios, as expected from theory, the splitting of the carbonyl, clearly evident in the carbon region (C=O and C=O···H at 287.6 and 288.7 eV, respectively), as it was with the silicon substrate, can now be also seen in the oxygen region (531.7 and 532.4 eV for nonbonded and hydrogen-bonded oxygen, respectively). Nitrogen is again present in one single state; its signal is at a BE of 400.1 eV, as expected. Moreover, the O 1s position at the binding energy of water adsorbed on gold, as predicted in the hydrogel spectra, has been definitively ascertained.

Therefore, these additional experiments have confirmed our assumption that amyloid formation is mediated by water hydrogen bonds, without any substrate influence, that involve both carbon and oxygen but not nitrogen.

However, it is also clear at this point that results from water suspensions cannot be directly related or cannot provide a simple explanation for the hydrogel results.
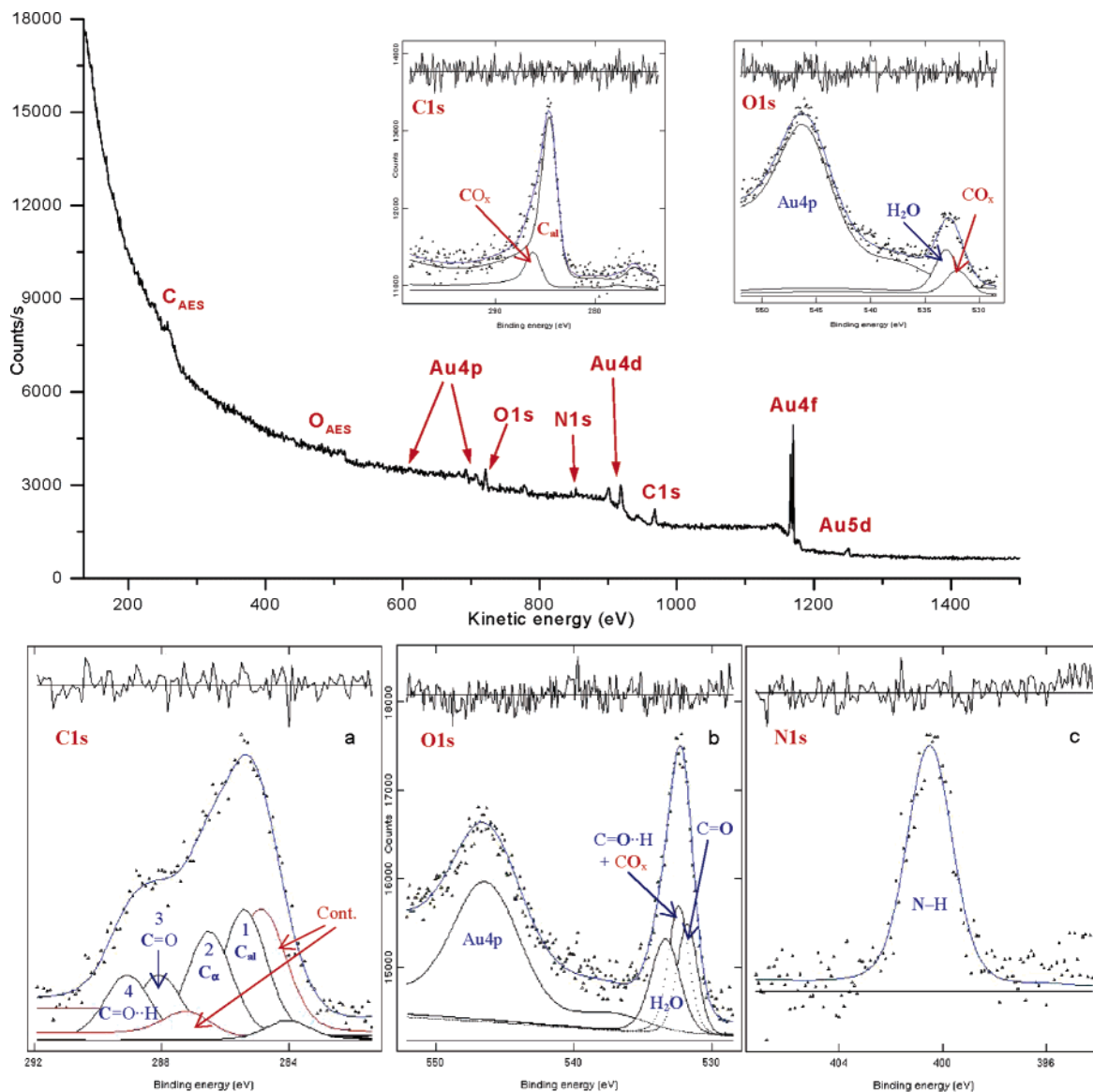
Figure 12. XPS wide scan of poly(ValGlyGlyValGly) suspended in water and deposited on gold: (a) C 1s, (b) O 1s, and (c) N 1s curve-fitted regions. The insets show C 1s and O 1s regions of the substrate before the deposition.

In the hydrogel experiments, deposition could be accomplished directly onto the sputtered gold substrate (with no extra oxygen) thanks to the hydrogel stickiness that allowed a uniform spread and covering of the whole area analyzed by XPS, and consequently, the only signals contributing to the O 1s region were from the polymer and water trapped within the polymer chains. There is no doubt from the hydrogel results that both carbon and oxygen belonging to carbonyl groups are well represented by only one chemical state. The problem, still to be addressed, is why the oxygen and the corresponding carbon shift differently when passing from their double chemical states in the suspension to the single state in the hydrogel.

A possible explanation can perhaps be attempted if we consider other forces such as dipole−dipole interaction playing a role in the formation of the hydrogel suprastructure: Their actions combined with the extensive hydrogen bonds would produce different effects on the two elements because of their different positions along the polymer chains. Also, it is worth remembering that for the same pentapeptide, in the monomer form, the binding energy of peptide carbon (also only one signal) was practically coincident with that of the hydrogel. There, computation provided explanations for the detection of only a

single XPS peak since, in fact, the spread in energy due to weak peptide hydrogen bonds was at the limit of our resolution.[7] Further experiments with monomer suspensions would probably provide clarifications, and certainly, also for the hydrogel, further validation of the given XPS chemical shifts by calculations would be of help. We can expect that the fractal dimension of the system, as revealed here, would probably simplify the approach for a theoretical modeling.

Conclusions

As reported in the literature[25−27] AFM has proved to be a powerful diagnostic tool with a promising role for the determination of mechanisms of amyloid growth.

Here, as in previous work,[7] we have shown how information from AFM images can be complemented by chemical analysis using XPS for a better description of such supramolecular mechanisms.

In particular, the transformation of amyloid fibers from aqueous suspension to hydrogel considers the following points:

• Poly(ValGlyGlyValGly) forms a uniform dispersion in water after a period of hydration.

• The fibers in the hydrogel are much smaller in diameter than in the initial deposit. They have a diameter of ca. 60 nm and a helical pitch of 80 nm. They are hollow and formed by spiralling of a flat ribbon with a thickness of between 6.5 and 10 nm and a width of 80 nm.

• It is possible that the fibers grow in length and uniformity by a process akin to reptation in which the strands on the surface move in a spiral motion.

• On the basis of XPS results, surface hydrogen bonds are much more uniformly distributed in the matured hydrogel structure than they were in the initial deposit. Certainly the fibers all experience the same environment given the one single state of the elements composing the peptide group even though their relative binding energies seem to indicate different bond strengths, thus implying, perhaps, other forms of interactions too.

• Also, the fractal dimensionality of the hydrogel is an important demonstration that the ELP here investigated has the property of self-similarity characteristic of the parent elastin, a fractal protein.[9,22]

As a whole, the results described in the present paper are strongly encouraging as far as the attainment of protein-based elastomeric biomaterials is concerned. Vascular prostheses, artificial cartilages, and so on could apparently be obtained, even by using recombinant DNA techniques and also by mimicking proteins such as abductin, resilin, spider silk, and other elastomeric proteins.

Finally, a uniform distribution of stiff, long fibers as those seen in the hydrogel images is reported in gelation processes occurring in human cells[28] and for plasma fibers that make up clots.[29] Knowing the molecular mechanism by which these networks form and the mechanical characteristics of each fiber composing the whole structure would have repercussions in many aspects of human life.

References and Notes

(1) Martino, M.; Perri, T.; Tamburro, A. M. Biopolymers and Biomaterials Based on Elastomeric Proteins. *Macromol. Biosci.* **2002**, *2*, 319−328 and references therein.

(2) Flamia, R.; Zhdan, P. A.; Martino, M.; Castle, J. E.; Tamburro, A. M. AFM Study of the Elastin-like Biopolymer (ValGlyGlyValGly). *Biomacromolecules* **2004**, *5*, 1511−1518.

(3) Tamburro, A. M.; Bochicchio, B.; Pepe, A. Dissection of Human Tropoelastin: Exon-By-Exon Chemical Synthesis and Related Conformational Studies. *Biochemistry* **2003**, *42*, 13347−1336.

(4) Debelle, L.; Tamburro, A. M. Elastin: Molecular Description and Function. *Int. J. Biochem. Cell Biol.* **1999**, *31*, 261−272.

(5) Tamburro, A. M.; Pepe, A.; Bochicchio, B.; Quaglino, D.; Pasquali-Ronchetti, I. Supramolecular Amyloid-like Assembly of the Polypeptide Sequence Coded by Exon 30 of Human Tropoelastin. *J. Biol. Chem.* **2005**, *280*, 2682−2690.

(6) (a) Kelly, J. W. The Alternative Conformations of Amyloidogenic Proteins and Their Multi-step Assembly Pathways. *Curr. Opin. Struct. Biol.* **1998**, *8*, 101−106. (b) Walsh, D. M.; Selkoe, D. J. Oligomers on the Brain: the Emerging Role of Soluble Protein Aggregates in Neurodegeneration. *Protein Pept. Lett.* **2004**, *11*, 213−228. (c) Dobson, C. M. Principles of Protein Folding, Misfolding and Aggregation. *Semin. Cell Dev. Biol.* **2004**, *15*, 3−16. (d) Sheibel, T.; Buchner, J. Protein Aggregation as a Cause for Disease. In *Molecular Chaperones in Health and Disease*; Gaestel, M., Ed.; Handbook of Experimental Pharmacology 172; Springer: New York, 2006; pp 199−219.

(7) Flamia, R.; Lanza, G.; Salvi, A. M.; Castle, J. E.; Tamburro, A. M. Conformational Study and Hydrogen Bonds Detection on Elastin-Related Polypeptides Using X-ray Photoelectron Spectroscopy. *Biomacromolecules* **2005**, *6*, 1299−1309.

(8) Castiglione Morelli, M. A.; De Biasi, M.; De Stradis, A.; Tamburro, A. M. An Aggregating Elastin-like Pentapeptide. *J. Biomol. Struct. Dyn.* **1993**, *11*, 181−190.

(9) Tamburro, A. M.; De Stradis, A.; D'Alessio, L. Fractal Aspects of Elastin Supramolecular Organization. *J. Biomol. Struct. Dyn.* **1995**, *12*, 1161−1172.

(10) *Fractals in Science*; Bunde, A., Havlin, S., Eds.; Springer-Verlag: Berlin, 1994.

(11) *Ulead Photo Express*, version 4.0 SE; Ulead Systems: 1992. http://www.ulead.com/pe/runme.htm (accessed March 2006).

(12) *Benoit, Fractal Analysis System*, version 1.01; TruSoft International: 1997. http://www.trusoft.netmegs.com (accessed March 2006).

(13) Peitgen, H.-O.; Jurgens, H.; Saupe, D. *Chaos and Fractals: New Frontiers of Science*; Springer-Verlag: New York, 1992; p 202.

(14) Barnsley, M. *Fractals Everywhere*; Academic Press: Boston, 1988; p 176.

(15) Mandelbrot, B. B. *The Fractal Geometry of Nature*; W. H. Freeman: San Francisco, 1983; p 91a.

(16) Falconer, K. *Fractal Geometry: Mathematical Foundations and Applications*; Wiley: Chichester, U. K., 1995; p 83.

(17) Castle, J. E.; Salvi, A. M. Chemical State Information from the Near-Peak Region of the X-ray Photoelectron Background. *J. Electron Spectrosc. Relat. Phenom.* **2001**, *114−116*, 1103−1113 and references therein.

(18) Castle, J. E.; Chapman-Kpodo, H.; Proctor, A.; Salvi, A. M. Curve-Fitting in XPS Using Extrinsic and Intrinsic Background Structure. *J. Electron Spectrosc. Relat. Phenom.* **1999**, *106*, 65−80.

(19) Shirley, D. A. High-Resolution X-Ray Photoemission Spectrum of the Valence Bands of Gold. *Phys. Rev. B* **1972**, *5*, 4709−4714.

(20) (a) *Practical Surface Analysis*; Briggs, D., Seah, M. P., Eds.; John Wiley and Sons: Chichester, U. K., 1990; Vol. 1, Appendix 6. (b) Seah, M. P. In *Practical Surface Analysis*; Briggs, D., Seah, M. P., Eds.; John Wiley and Sons: Chichester, U. K., 1990; Vol. 1, Chapter 5.

(21) *Surface Analysis by Auger and X-ray Photoelectron Spectroscopy*; Briggs, D., Grant, J. T., Eds.; IM Publications: Chichester, U. K., 2003.

(22) Tamburro, A. M.; Daga-Gordini, D.; Guantieri, V.; De Stradis, A. On the Molecular and the Supramolecular Structure of Elastin. In *Chemistry and Properties of Biomolecular Systems*; Russo, N., Anastassopoulou, S., Barone, G., Eds.; Kluwer: Dordrecht, The Netherlands, 1994; Vol. 2, pp 389−403.

(23) Castle, J. E.; Salvi, A. M.; Guascito, M. R. Substrate-Related Feature in the Loss Structure of Contamination C 1s. *Surf. Interface Anal.* **1999**, *27*, 753−760.

(24) Ball, P. Life's Matrix: Water in the Cell. *Cell. Mol. Biol.* **2001**, *47*, 717−720.

(25) Kad, N. M.; Myers, S. L.; Smith, D. P.; Smith, D. A.; Radford, S. E.; Thomson, N. H. Hierarchical Assembly of β_2-Microglobulin Amyloid In Vitro Revealed by Atomic Force Microscopy. *J. Mol. Biol.* **2003**, *330*, 785−797.

(26) Lashuel, H. A.; LaBrenz, S. R.; Woo, L.; Serpell, L. C.; Kelly, J. W. Protofilaments, Filaments, Ribbons and Fibrils from Peptidomimetic Self-Assembly: Implications for Amyloid Fibril Formation and Material Science. *J. Am. Chem. Soc.* **2000**, *122*, 5262−5277.

(27) Calamai, M.; Canale, C.; Relini, A.; Stefani, M.; Chiti, F.; Dobson, C. M. Reversal of Protein Aggregation Provides Evidence for Multiple Aggregated States. *J. Mol. Biol.* **2005**, *346*, 603−616.

(28) Day, C. Single, Physics-Based Model Accounts for the Mechanical Properties of Diverse Biopolymer Gels. *Phys. Today* **2005**, *58* (7), 27−29.

(29) Robinson, K. Laser Trap Stretches Blood Clot Fibres. *Biophotonics Int.* **2005**, *12*, 28−29.